Eur. Phys. J. D **22**, 31–40 (2003)
DOI: 10.1140/epjd/e2002-00221-1

THE EUROPEAN PHYSICAL JOURNAL D

Study of the stability of beam characteristics of the neon-like Zn X-ray laser using a half cavity

A.R. Präg[1,a], T. Mocek[1], M. Kozlová[1], B. Rus[1], G. Jamelot[2], and D. Ros[2]

[1] Inst. of Physics, Academy of Sciences of the Czech Republic, Na Slovance 2, 18221 Prague 8, Czech Republic
[2] LIXAM, Bâtiment 350, avenue Jean Perrin, Université Paris-Sud, 91405 Orsay, France

Received 17 May 2002 / Received in final form 10 September 2002
Published online 6 November 2002

Abstract. At the Prague Asterix Laser System Center (PALS) the Asterix iodine laser delivering up to 700 J/0.5 ns is used as a pump source for X-ray laser experiments and applications. The prepulse technique was applied which is known to improve the neon-like X-ray laser output at the $J = 0-1$ transition dramatically. Since Zn slab targets were used the operating wavelength was 21.2 nm. A prepulse having up to 20 J precedes the main pulse by 10 ns. The main beam and the prepulse beam are focussed by two different optical systems separately and their foci are superimposed at the target surface. By implementing a half-cavity set-up for double-pass amplification using a Mo/Si multilayer mirror – which can be used for more than 100 shots – the X-ray laser output was more than 10 times stronger than at the single pass in a 30 mm long plasma. Double-pass amplification was observed to be most efficient when the pump pulse duration was at least 150 ps longer than the round trip time ($\approx$ 260 ps) in the half-cavity. Under this fundamental condition the X-ray laser reached saturation in the double-pass regime containing approx. 4 mJ energy which has been proved to be enough for future applications. In this contribution, the X-ray laser features like divergence in two dimensions, the beam quality (symmetry), the pointing angle and the integrated intensity giving an estimation of the output energy are investigated over 110 shots. To characterize the stability of the X-ray laser the shot distribution, the mean value and the standard deviation for these parameters are evaluated. For 18 shots in a series – what was achievable during one day – the corresponding values are given, and a statistical analysis carrying out a chi-squared test characterize the Zn X-ray laser as a robust tool suitable for applications. In the future it is planned to allocate X-ray laser beam time to external research groups.

PACS. 42.55.Vc X- and γ-ray lasers – 42.60.Da Resonators, cavities, amplifiers, arrays, and rings – 42.60.Jf Beam characteristics: profile, intensity, and power; spatial pattern formation – 52.50.Jm Plasma production and heating by laser beams (laser-foil, laser-cluster, etc.)

1 Introduction

The development of X-ray lasers (XRL) has been reported in the past several years [1,2]. Several approaches were verified experimentally in a couple of laboratories [1]. Historically the first approach used collisional excitation of Ne- and Ni-like ions shortly later. Intense lasing over a broad wavelength range was realised by using pump pulses of 500 ps down to less than 100 ps. XRL at wavelengths of 15.5, 20.6, 23.6, 21.2, 23.1, 25.5 and 28.5 nm in Ne-like Y, Se, Ge, Zn, Ni, Fe, and Cr [3–12] and at 5.8, 7.3 and 13.9 nm in Ni-like Dy, Sm, and Ag [10,11] were demonstrated. Output energies of 7 mJ in Ne-like Y [5] and recently several mJ in Ne-like Ni [12] were reported. A modification of the pumping method is the transient collisional excitation (TCE) involving travelling wave excitation. Using TCE lasing has been reported at 32.6 and 19.6 nm in Ne-like Ti and Ge [13,14], and at 7.3 11.9, 13,9, 14.7, and 18.9 nm in Ni-like Sm, Sn, Ag, Pd, and Mo [15–18]. A second approach to generate XRL is based on a capillary-discharge system where the lasing medium is in a gas-filled capillary driven by a fast high-current pulse. Strong lasing at 46.9 nm in Ne-like Ar has been demonstrated with this method [19,20]. A third approach is based on optical-field ionisation by ultrashort laser pulses and employs a longitudinally pumped gas cell. Using this method lasing at 41.8 nm in Pd-like Xe [21] was published.

In this work we use the prepulse technique which is known to improve the $J = 0-1$ lasing dramatically [22]. We examine the performance of double-pass amplification at 21.22 nm in Ne-like zinc, using a 3 cm long plasma and a half-cavity set-up. Intense lasing in zinc has been demonstrated [23], and later the essential role of weak prepulses (0.01 to 0.1% of pump energy) was identified [24,25]. Saturated operation of the $J = 0-1$ zinc laser using a half-cavity configuration was realised [23] and has been characterised in detail [25].

[a] e-mail: praeg@fzu.cz

The widely diversified application of XRL is coupled to the condition of an appropriate stability of the pulsed XRL beam. The stability of XRL beam parameters (*e.g.* beam size, divergence, symmetry, pointing angle, energy, coherence and pulse duration) was to our knowledge, up to now not investigated in some detail over a long series of shots. For the practical point of view, in order to use XRL for applications it is interesting to have not only a high-repetition rate but also a high degree of reproducibility from shot to shot. Mostly in literature there are presented single-shot results, especially by using long-pulse systems at low repetition-rate. However, in some publications a considerable shot-to-shot fluctuation was reported [26,27], although without analysing the underlying reasons in detail. For the Ar capillary-discharge XRL Benware *et al.* [26] reported on the laser output intensity fluctuations over nine consecutive shots using the same capillary. The observed intensities scattered over a factor of three. The scattering of the XRL beam divergence and deflection angle was investigated by Kuba *et al.* [27] for the TCE nickel-like Ag laser evaluating altogether 15 shots. To our knowledge, for short-pulse systems shooting at a Hz-rate, there is no statistical analysis of the fluctuations published up to now, too. Despite possible reasons for the fluctuations like pump laser instabilities (scattering of pulse duration and shape, degradation of optical components due to damage, et cetera) in this contribution we study the stability over 110 shots, at a low repetition-rate of 20 up to 30 minutes between two shots. Nevertheless, the low rep-rate constitutes a considerable disadvantage for the statistical analysis, because the confidence into statistics is increasing with the size of the random sample achieved on a practicable time-scale.

Typical values for the beam quality of single-shots reported in the literature are 1.3 and 3.7 mrad for the nickel-like Sn XRL divergence perpendicular to the target surface ("*horizontal*") and parallel to the target surface ("*vertical*"), respectively [28]. For nickel-like silver the divergences are investigated as a function of the focal line width in [29] where divergences between 2.2 and 3 mrad (horizontal direction) and between 5 and 6 mrad (vertical direction) are reported. Generally for the vertical divergence a higher value was measured than for the horizontal divergence [1]. Defining a dimensionless parameter, that we will call the *beam symmetry* as the ratio of horizontal to vertical divergence, a value considerably smaller than 1 was published. This result is due to the asymmetric plasma expansion in either direction (parallel or perpendicular to the target surface). Due to the same context from two-dimensional near-field images of nickel-like Mo [18] and neon-like Ge and Ni [30] XRL can be extracted that the gain region in the ionised plasma is in the direction parallel to the target considerably larger than in the perpendicular direction.

Two-dimensional far-field patterns are reported by Moreno *et al.* [31], Fourcade *et al.* [32], and Tang *et al.* [29]. Double-pass amplification applying a two-target geometry [33,34] or using a half-cavity was reported earlier in [25]. Applying time-resolving measurements pulse durations between 70 ps [23] and 100 ps [25] for the neon-like Zn XRL are reported. However, the pulse duration stability over sub-sequent shots was, to our knowledge, still not investigated.

The primary goal of this contribution is to demonstrate that a half-cavity zinc XRL containing at the output a few millijoules, pumped by a 600 J/450 ps drive laser, has an excellent stability in the beam quality in a series of more than 100 shots thus representing a robust tool suitable for applications. On the other hand it is also shown that just one multi-layer mirror may be used for more than 100 subsequent shots without re-aligning the half-cavity and without opening the vacuum chamber. Potentially this allows a higher shot rate if a high-repetition pumping system is available.

We investigate the beam stability of a double-pass amplified XRL under the condition that the prepulse level and the half-cavity geometry are only slightly varied. The shot-to-shot fluctuations of the beam divergence, symmetry, and pointing angles are explored statistically. The obtained results are discussed using a chi-squared fitting test procedure [35] in a primary hypothesis assuming that the observables are Gaussian (randomly) distributed.

2 Experimental set-up

The experiments were performed at the PALS (Prague Asterix Laser System) Center [36], where the high-power iodine laser ASTERIX, developed originally at the Max-Planck-Institute für Quantenoptik (Garching) was installed and set into operation in autumn 2000 [37]. This laser using five amplifier stages is capable of delivering 700 J beam energy in a 0.5 ns pulse and is therefore suitable to pump soft X-ray lasers efficiently. The laser is operated at the fundamental wavelength of 1 315 nm. A scheme of the experimental set-up including the mainly used components is shown in Figure 1. In order to produce a suitable line focus two completely new focusing optics were constructed and assembled in front of the entrance windows of the spherical target chamber [36]. The main beam of 290 mm diameter is focussed by using an aspherical lens of 1.06 m focal length combined with a cylindrical lens matrix consisting of 10 concave cylindrical lenses. The resulting line focus has a length of 30 mm and a width of approximately 130 μm. As described in detail in [38] the cylindrical lens matrix is arranged as two arrays [39] of five lenses mounted in a support including a 10-mm high horizontal strut at the central array border, protected from the laser by a stripe of high-absorbing glass of 5 mm thickness. The prepulse beam which is extracted after the fourth amplifier has a diameter of 148 mm and is guided separately to the target chamber delivering up to max. 100 J and having identical pulse duration like the main pulse. Using a second focusing optics consisting of a spherical lens (focal length 1.5 m) and a single convex cylindrical lens the prepulse beam is focussed onto the target at an angle of 25 degrees in relation with the normal incident main beam (Fig. 1). The independent focusing of main pulse and prepulse has the unique advantage

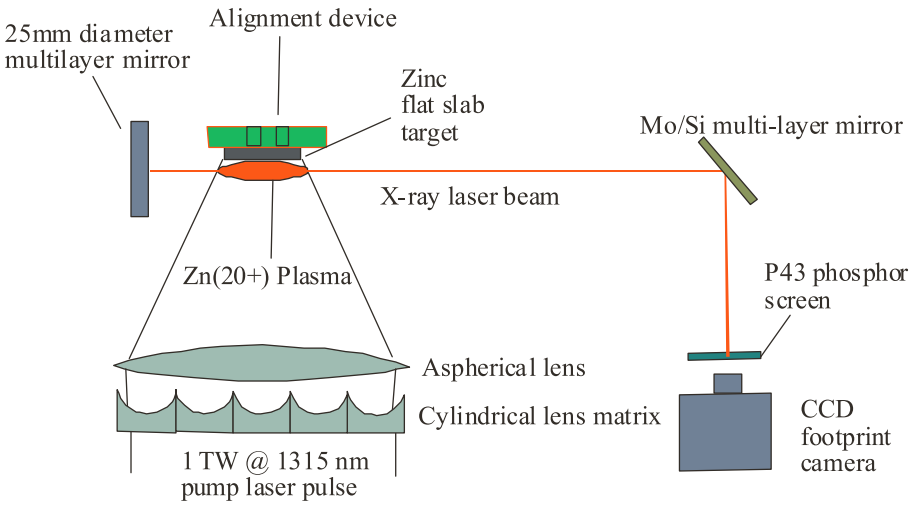

Fig. 1. Scheme of experimental set-up (not in scale). The line foci of the prepulse and mainpulse are superimposed at the target surface. The half-cavity mirror is located 8.5 mm from the target edge. A hair-cross in front of the footprint screen is serving as a fiducial.

that the both corresponding line foci can be modulated separately. Thus the 35-mm long prepulse line focus was slightly defocused to a width of approximately 700 μm, so that the center of the pre-plasma prepared for the main pumping pulse is as uniform as possible. The superposition of both line foci can be controlled at each shot by using an off-axis X-ray pinhole camera. The pinhole camera is imaging the incoherent X-rays in the keV region radiated from the plasma. The lateral width and uniformity of the plasma column can be monitored by this camera in which an off-shelf CCD chip combined with a 3 μm Al filter is employed as the detector.

In order to realize an adjustable delay between the prepulse and the main pulse a delay-line was accommodated in the laser hall of PALS so that the corresponding optical path lengths allow the variation of delays between 0.5 ns and 20 ns. For the experiments reported in this paper a delay of 10 ns was employed. The delay was controlled by a monitor constructed recently by using two fast InGaAs photo diodes sensitive in the infrared (IR). One is used for the mainpulse, the other one for the prepulse by inserting different absorption filters. The time difference between the two signal rising edges was measured on an oscilloscope with 3 GHz bandwidth (Tektronix TDS 694C) thus giving the delay at every shot. This prepulse monitor is able to detect parasitic prepulses of the pump laser, however this could be excluded during our experiments in general.

The targets were optically polished, flat Zn slabs having a surface flatness about 5 μm or better and a width of 30 mm. The Zn purity was better than 99.9%. One 5-cm high target may be used for more than 100 shots, when it is shifted vertically by 300 μm after each shot to irradiate fresh target surface in the subsequent shot. The target is bonded on an interchangeable support plate, of which the position with respect to the focal plane can be controlled very precisely.

For the realization of the half-cavity set-up we used flat Mo/Si multi-layer mirrors having a layer period of approx. 11 nm and a diameter of 25 mm. The mirrors were produced by the Institute of Scientific Instruments in Brno, Czech Republic. At the wavelength of 21.2 nm a reflectivity of approx. 30% was measured at normal incidence [38]. The half-cavity mirror is shown in Figure 2 where the small spots of damages after 63 shots are clearly seen. The still clean surface area illustrates that the mirror can be used for a number of shots additionally. The distance between multi-layer mirror and target edge was 8.5 mm. The mirror was mounted in a fully-automated motion system allowing five degrees of freedom for mechanical motions, like moving, tilting and rotating, respectively. The re-injection angle around the vertical axis, *e.g.*, could be varied between -10 and $+10$ mrad in relation to the target surface. The un-used mirror surface was protected by a 1-mm thick stainless-steel shield having a pinhole of 1 mm diameter as a gap for the X-ray laser beam. Since at each shot the mirror surface was damaged in a 1-mm spot the mirror will be moved behind the protection shield by 2 mm parallel to the surface without changing the position of the pinhole. By applying this procedure more than 100 shots are possible with only one mirror. The mirror motion system was mounted within the vacuum chamber and was controlled by a PC fully automatically. A breaking of the vacuum (10^{-3} Pa) due to an opening of the chamber is not necessary.

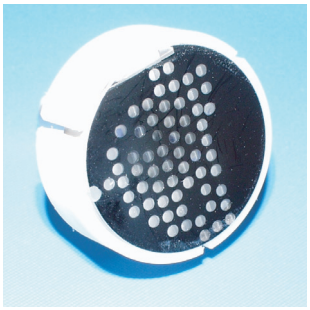

Fig. 2. The half-cavity multilayer mirror after finishing the experiments. It was used for 63 shots leaving 63 small spot damages of $\approx$ 1 mm diameter. The clean area can be used later.

The emerging XRL beam may be alternatively analysed by an X-ray spectrometer, or by a footprint monitor or may be sent to an X-ray interferometer. The beam is switched between the individual diagnostics by the means

of a flat retractable Mo/Si multilayer mirror working at 45 degrees reflection angle.

As primary diagnostics a time-integrating spectrometer employing Wadsworth geometry was used [40]. The spectrometer consists of an on-axis curved blazed grating with 900 lines per mm (radius of curvature 4675 mm) and a phosphor screen of 40 mm diameter coupled to a Peltier-cooled CCD (Photonic Science, East Sussex, UK). The radius of the Wadsworth circle is 1.2 m. The grating is working at the grazing incidence angle of approximately 15 degrees. The phosphor screen is mounted tangentially on the Wadsworth circle thus the spectrally resolved radiation is detected under a flat angle of 10 degrees. To avoid saturation of the detector at half-cavity shots we inserted an Al filter of 1.5 μm thickness into the beam path, having a transmission of 11% at 21.2 nm.

Alternatively, a second diagnostics is detecting a two-dimensional far-field pattern (footprint) of the X-ray laser beam. Taking the dimensions of the footprint the measurement of the beam divergence parallel and vertical to the target surface is realized. The X-ray beam is reflected by a Mo/Si multi-layer mirror (optimised for 45 degrees reflection angle) perpendicularly onto a phosphor screen of 38 mm diameter. The path length from the target to the phosphor *via* the mirror is 1.1 m. The fine-grain phosphor screen (grain-size 1−3 μm) manufactured by Proxitronic (Bensheim, Germany) is a Gd_2O_2S:Tb (P43) aluminised with a 50-nm thick layer, thus not sensitive for radiation in the visible and in the infrared. Additionally the phosphor is protected against scattered light by a 20-cm long metal tube in front of it thus only the radiation reflected by the multi-layer mirror is illuminating the phosphor. The footprint on the phosphor is recorded by a standard CCD working in the visible. A hair-cross consisting of 120-μm-diameter wires was put as a spatial fiducial into the X-ray beam path positioned 22 cm in front of the phosphor.

The experiment is carried out considering the following order. The prepulse level is fixed at a level optimised for single pass output as monitored by the time-integrating spectrometer. Subsequently the half-cavity output is studied by changing slightly the half-cavity geometry, *i.e.*, the multi-layer mirror reflecting the beam back into the gain region is tilted at very small angles of few mrad [38]. Finally the beam quality is investigated by using the footprint diagnostics. Simultaneously, at any shot the pump laser energy is measured.

3 Experimental results

The experimental results presented here were obtained using a 1.6 J prepulse, followed after 10 ns by the typical 500-J main pulse producing a target irradiance of $\sim 2.8 \times 10^{13}$ Wcm^{-2}. Taking into account the prepulse focus width of $\sim$700 μm, the prepulse irradiance was $\sim 1.6 \times 10^{10}$ Wcm^{-2} which corresponds to a prepulse/mainpulse irradiance ratio of $\sim 6 \times 10^{-4}$. We note that this observation of a very weak prepulse optimising a zinc laser corroborates the former results obtained by MacPhee *et al.* [42].

The laser signal at 21.2 nm was completely dominating the X-ray spectrum, thus due to the very weak (negligible) background it was possible to make two-dimensional far-field patterns (footprints) of the X-ray laser beam solely.

A footprint of the ASE X-ray beam emergent from a 3-cm long plasma is shown in Figure 3, along with its intensity profiles. A smooth ellipsoidal beam possessing a high symmetry is produced having the horizontal divergence of 3($\pm$0.5) mrad and the vertical divergence of 5($\pm$0.5) mrad, respectively. This is giving a beam symmetry of 0.6. The beam is emitted from the plasma under a deflection angle of 5.5($\pm$0.5) mrad with respect to the target surface. This pointing angle was observed to be almost identical in all single-pass shots.

Upon activating the half-cavity mirror, the X-ray laser output from a 3-cm plasma is enhanced typically by one order of magnitude, so it was necessary to reduce the aperture of the footprint CCD, what has no influence onto the beam divergence measurement.

Considering the round trip time of 257 ps in the half-cavity it is emphasised that the half-cavity is working efficiently only under the fundamental condition, that the pump pulse duration is at least 150 ps longer than the round trip time [38]. For pulses shorter than $\sim$400 ps it is not guaranteed that the inversion is lasting sufficiently long for amplification during the whole round trip. Due to this context the distance between the half-cavity mirror and the target was put to 8.5 mm, the minimum feasible at the experimental set-up.

Figure 4 displays a footprint record of the double-pass beam emitted in the optimum half-cavity configuration at the re-injection angle of 3 mrad [38]. The beam emerges from the plasma under an angle of $\sim$5 mrad and its horizontal and vertical divergence of 3.8($\pm$0.5) and 5.8($\pm$0.5) mrad, respectively, and thus the beam symmetry of 0.65 are close to those of the single pass ASE. The statistical analysis carried out in the following is using the shots when the investigated zinc XRL is operated in double-pass amplification, exclusively.

The histograms in Figure 5 show the distributions of the XRL beam divergence in horizontal (a) and vertical (b) direction observed at 18 sub-sequent half-cavity shots. The number related to each interval gives the measured frequency. Introducing a dimensionless parameter calculated as the ratio of horizontal to vertical beam divergence we make a simple definition of the beam symmetry. The histogram in Figure 6a represents the distribution of observed beam symmetries. For comparison the distribution of the measured pump laser energies for the same shots is depicted in Figure 6b. The obvious and remarkable difference of both distributions is analysed and discussed in the following sections.

4 Chi-squared test and statistical analysis

The X-ray laser output generated both by the single and the double pass was observed to be largely robust with respect to a large number of shots. It equally exhibited

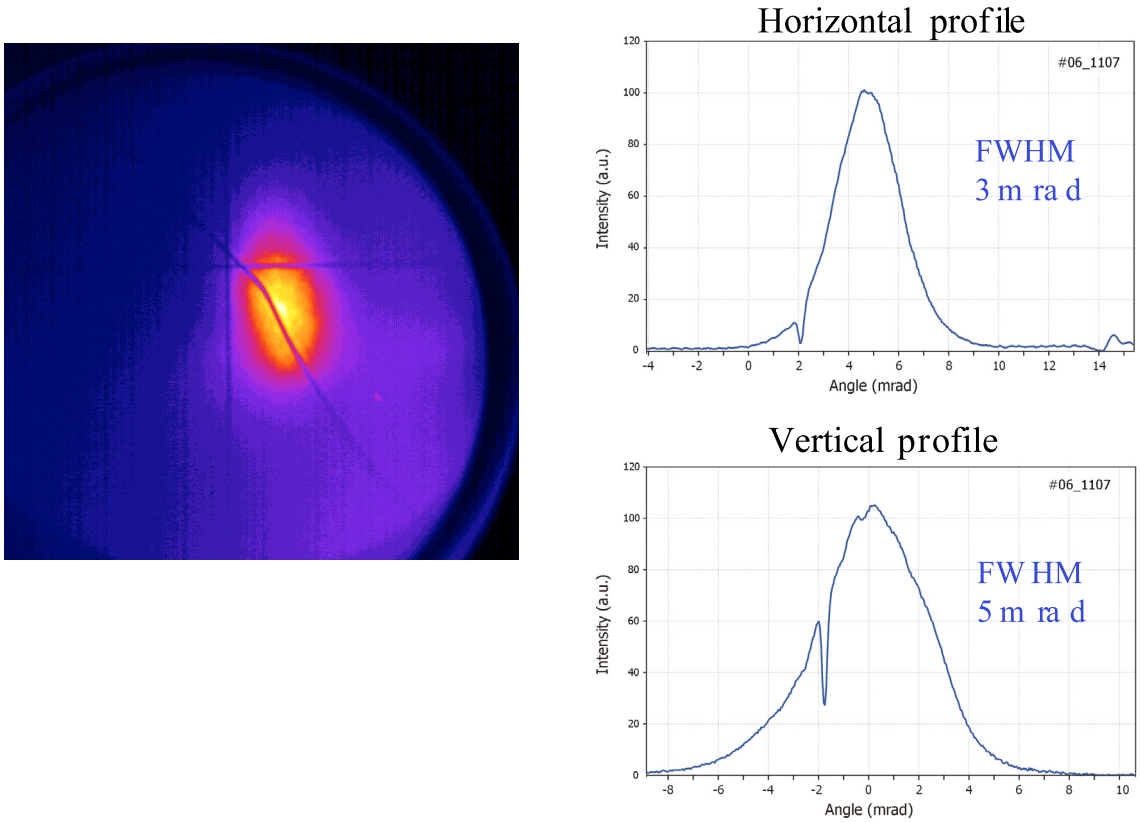

Fig. 3. Far-field pattern (footprint) of the 21.2-nm XRL beam produced in the single-pass, with its horizontal and vertical scans. The target surface is on the left side of the footprint.

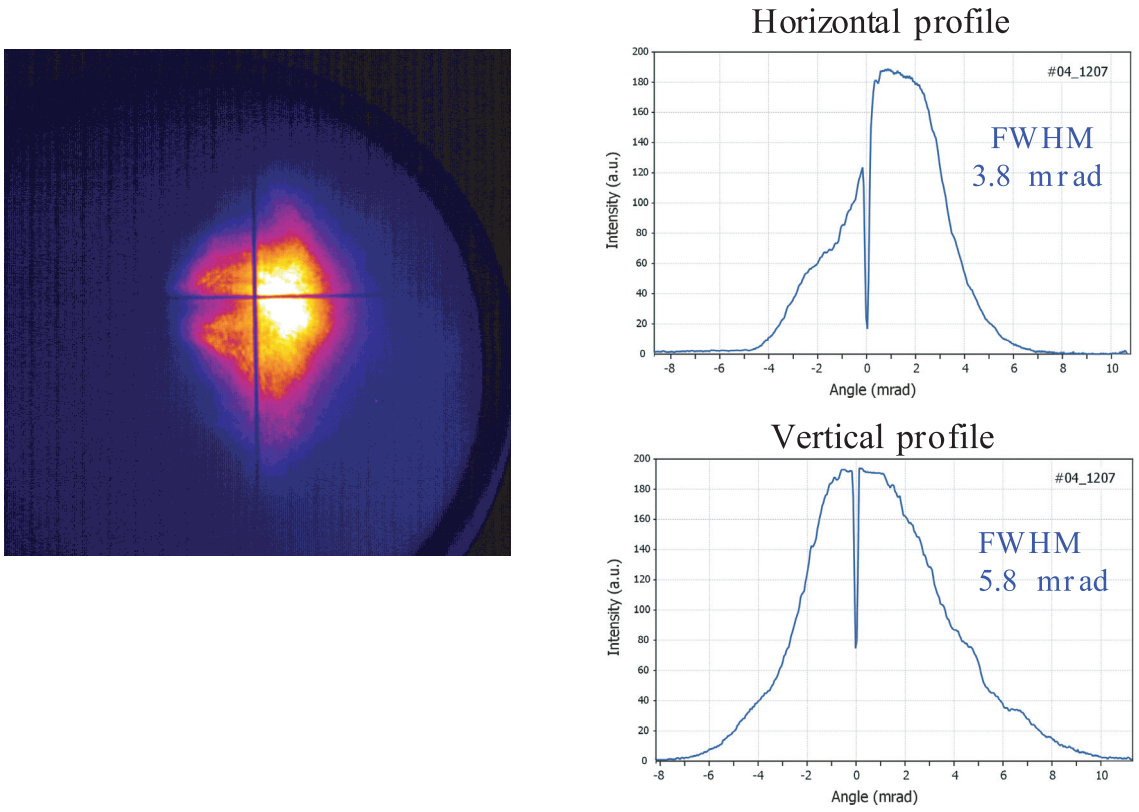

Fig. 4. Footprint of the double-pass amplified 21.2-nm XRL beam, together with its horizontal and vertical profiles. The target surface is on the left side. The fiducial wires are seen as narrow-lined shadows on the footprint.

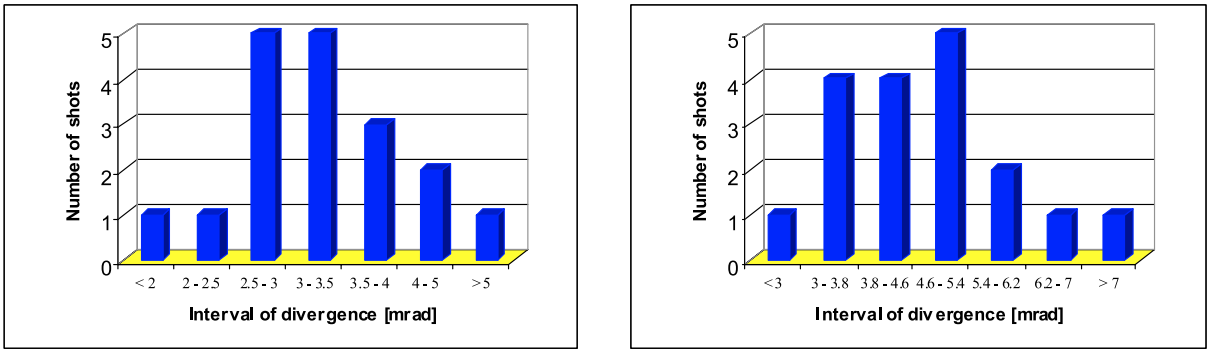

(a) horizontal (b) vertical

Fig. 5. Histogram representing the distribution of the beam divergence in horizontal (a) and vertical (b) direction as measured in units of mrad.

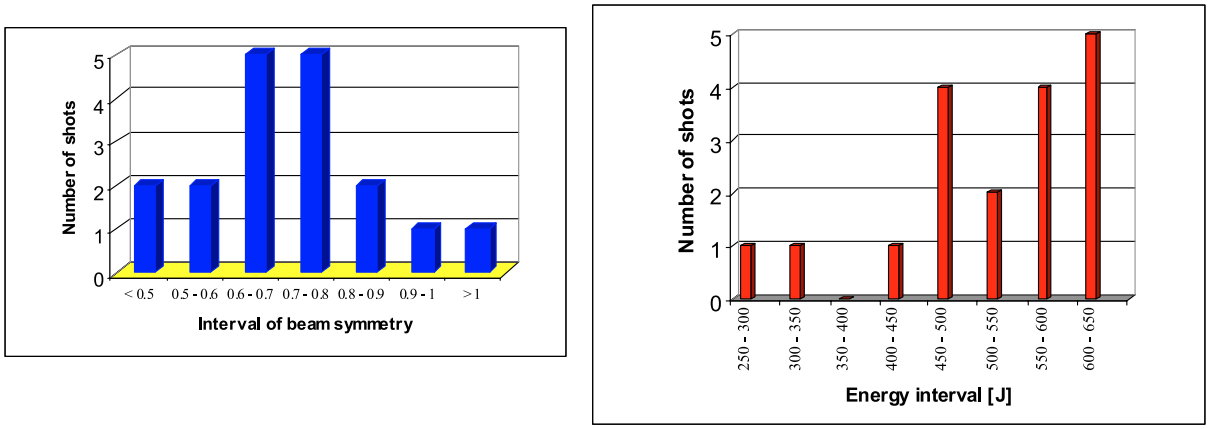

(a) XRL beam symmetry (b) Pump laser energy

Fig. 6. Histogram (a) illustrating the distribution of the XRL beam symmetry defined as the ratio between horizontal and vertical divergence. For comparison the pump laser energy distribution according to the same shots is shown in (b).

an excellent reproducibility after an exchange of the Zn target and of the half-cavity mirror.

In the following we are executing a statistical analysis of the experimental results including a chi-squared test which is used as a common tool for controlling the quality and reliability of products or processes.

The procedure of a chi-squared fit test is described elsewhere [35]. At the beginning we are making a hypothesis of the underlying distribution. As a hypothesis we assume a Gaussian distribution. The assumption of a Gaussian (normal) distribution makes sense in all measurements at which the experimental errors are randomly distributed and independent of other controllable parameters. The observed fluctuations are considered to have statistical reasons. Possible systematical errors (target preparation, alignment, temperature fluctuations etc.) are not investigated here.

In three steps we can perform the chi-squared test:

1. we define several intervals and assign the experimental results to these intervals ("*classes*"). Taking into account the number of estimated values defining the intervals then the degrees of freedom are given therefore;
2. by using the hypothesis of an expected distribution we can calculate the chi-squared value from the test using the formula (1);
3. we compare the chi-squared value with the values given in a probability table [43] and extract a probability of making no error by accepting or rejecting the hypothesis. The probabilities printed in statistical tables [43] are calculated by using equation (5).

It is emphasised that the test is not telling whether the hypothesis is true or not, it is only giving a probability to accept or to reject the hypothesis. Besides, in the case of rejecting the hypothesis the test is not explaining the reasons for doing that. In the case the hypothesis will be accepted the test is delivering a probability for the chance of making an error, anyway.

The χ^2 is a measure of the deviation between the observed distribution (Figs. 5 and 6) and the expected, in our case, Gaussian distribution

$$\chi^2 = \sum_{i=1}^{k} \left(\frac{(m_i - Np_i)^2}{Np_i} \right) \tag{1}$$

where k is the number of classes (intervals), m_i is the observed number of shots in the ith interval (*the measured*

frequency), p_i is the expected probability of the ith interval, and N is the total number of all shots investigated.

We begin the statistical analysis in determining the mean value and the standard deviation of all measured values. The arithmetic mean value or average a is given by the sum of all measured values S_i divided by N, the total number of shots. The standard deviation s as the square-root of the variance is given by equation (2):

$$s = \sqrt{\frac{1}{N-1}\sum_{i=1}^{N}\Big((S_i - a)^2\Big)}. \tag{2}$$

The probability p_i to find a result lying in the ith interval can be expressed as

$$p_i = \left(\frac{1}{\sqrt{2\pi(s)^2}}\right)\int_{L_i}^{H_i}\Big(\exp\Big(-(x-a)^2/2(s)^2\Big)\Big)\mathrm{d}x \tag{3}$$

where L_i and H_i denote the lower and upper limits of the ith interval, respectively. Equation (3) is due to our expectation of a Gaussian distribution. The expected frequency at the ith interval is Np_i.

Choosing appropriate limits L_i and H_i we define seven intervals (Tab. 1), we count the number of experimental hits (*frequency*) in each interval, and we find the degrees of freedom of the chi-squared test.

The degrees of freedom f are defined as $f = k - 1 -$ (number of estimated parameters). In our case with 7 intervals and two estimated parameters for the mean value and the standard deviation we get $f = 4$.

The density function of the chi-squared distribution is generally given as

$$d = \left(\frac{1}{2^{\frac{f}{2}}\Gamma(f/2)}\right)\exp(-y/2)y^{\frac{f}{2}-1} \tag{4}$$

using the substitution $y := \chi^2$ for simplification. Γ denotes the well-known gamma-function.

Integration of the density function d leads to a probability β for rejection of the hypothesis according to equation (5). This probability β can be expressed as

$$\beta = \left(\frac{1}{2^{\frac{f}{2}}\Gamma(f/2)}\right)\int_0^{\chi^2}\Big(\exp(-y/2)y^{\frac{f}{2}-1}\Big)\,\mathrm{d}y \tag{5}$$

where the upper integration limit χ^2 is given by equation (1). At fixed f with higher χ^2 the probability β for rejection will be enlarged.

In our case ($f = 4$) the integration can be solved analytically and using $y := \chi^2$ we receive

$$\beta = 1 - \frac{1}{2}(2+y)\exp(-y/2). \tag{6}$$

The probability due to the acceptance of the hypothesis is $\alpha = 1 - \beta$. With extended χ^2 the probability α for acceptance will be smaller and *vice versa*.

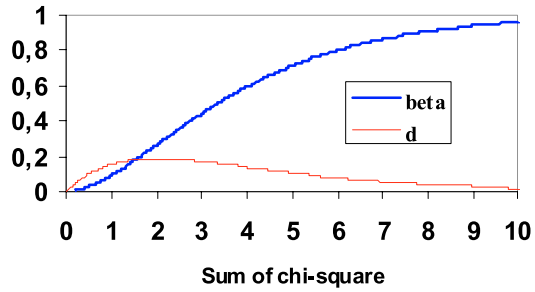

Fig. 7. Density function and probability of the chi-squared distribution for four degrees of freedom.

The density function $d(\chi^2,\ f = 4)$ and the probability function $\beta(\chi^2,\ f = 4)$ are plotted in Figure 7 for our case of $f = 4$ degrees of freedom.

In the case χ^2 is above the threshold (*critical value*) the hypothesis should be rejected. In the opposite case the hypothesis can be accepted since the result of the chi-squared test is not in contradiction to the hypothesis.

Customarily there is set a statistical significance level (*critical probability level for rejection*) above that the hypothesis will be rejected. It can be for example $\beta = 0.50$ (half-to-half) or $\beta = 0.95$ (usually). In the latter case there is an error of less than 5% when the hypothesis is rejected. For $f = 4$ degrees of freedom the corresponding χ^2 thresholds are $\chi^2 = 3.357$ ($\beta = 0.50$) and $\chi^2 = 9.488$ ($\beta = 0.95$), respectively. Particularly when the sample is rather small (less than 100) or the number of shots in some of the intervals is less than 3, this can lead to an over-estimation of χ^2 and thus to an under-estimation of the acceptance probability α. Thus in our test we will not accept the hypothesis careless. It is clear that the statistics will be improved with increasing number of shots. Therefore in the future it is necessary to broaden the statistical data available.

5 Statistics of the XRL beam quality

The mathematical tool of the chi-squared test we apply onto the X-ray laser beam parameters. Table 1 gives the execution of the chi-squared test as an example for the beam symmetry of the half-cavity XRL observed in a series of 18 shots.

The sum of the values in the final column of Table 1 gives the $\chi^2 = 1.396$. Using equation (6) we calculate $\beta = 0.156$ and $\alpha = 0.844$.

Instead of performing the on principle same procedure for the vertical beam divergence, as well as for horizontal divergence we summarise the corresponding results for all these beam properties observed at several shots in Table 2.

We discuss now our chi-squared test results. Concerning the beam symmetry, the horizontal and the vertical divergences χ^2 and β are less than the critical values: the hypothesis will be accepted, because there is no statistical significance for rejection. On the other hand in the case of rejection we would have a probability error of more than 55% for these beam parameters as given in Table 2. This is

Table 1. Parameters of the chi-squared test for the beam symmetry of the Zn XRL evaluated from a one-day experiment.

Class number i	Interval limits L_i, H_i	Observed frequency m_i	Expected frequency Np_i	$(m_i - Np_i)^2/Np_i$
1	less than 0.5	2	2.20	0.02
2	0.5–0.6	2	2.75	0.21
3	0.6–0.7	5	3.83	0.35
4	0.7–0.8	5	3.90	0.31
5	0.8–0.9	2	2.90	0.28
6	0.9–1.0	1	1.57	0.20
7	more than 1.0	1	0.85	0.03

Table 2. Statistical parameters and results of chi-squared tests for the beam properties of the Zn XRL evaluated from a one-day experiment.

	horizontal divergence	vertical divergence	beam symmetry
Number of shots	18	18	18
Average a	3.43 mrad	4.77 mrad	0.75
Standard deviation s	0.92 mrad	1.31 mrad	0.25
Sum of χ^2	3.03	2.03	1.40
Probability $\alpha = 1 - \beta$	0.55	0.73	0.84

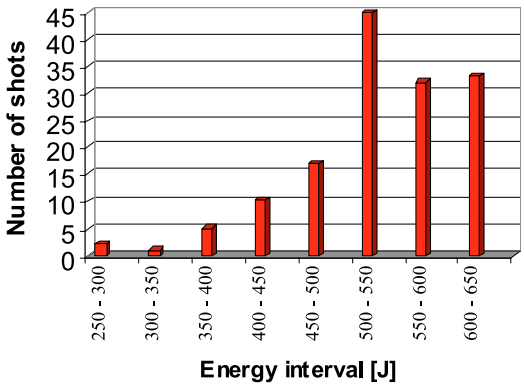

Fig. 8. Histogram showing the distribution of the Asterix pump laser energy extracted during a two weeks project when using all five amplifier stages.

the only argument to accept the hypothesis. It is not clear, whether the hypothesis is really true. But from the statistical point of view the Gaussian (normal) distribution seems to be a reasonable assumption.

The opposite case would be if χ^2 resp. β are higher than critical value: then the hypothesis would be rejected and the error probability for doing that is less than α%. This case is not fulfilled here.

Considering the beam divergences in two dimensions and the beam symmetry there is no statistical significance to reject the hypothesis of a Gaussian distribution.

A possible objection that the chi-squared test is favouring the acceptance of our hypothesis of a Gaussian distribution can be enfeebled by analysing the pump laser energy fluctuations, for example. As shown in Figure 8 the pump laser energy is varying between 270 J and 640 J and the considerable asymmetric-shaped distribution is far away from a normal distribution. We extract a mean pump energy of 523 J and a standard deviation of 97 J. A chi-squared test having $f = 5$ degrees of freedom gives for this example values of $\chi^2 = 22.7$, thus $\beta = 0.999$ and α is less than 0.1%, respectively. According to the critical threshold in this case the hypothesis of a normal distribution must be rejected obviously. The pump energy is definitely not random-distributed. That means that the XRL fluctuations are considerably smaller than the scattering of the pump laser output. This fact exhibits a supplementary confirmation that the double-pass amplified Zn XRL is working in deep saturation what is stabilising the XRL output apparently. As evaluated in [38] the observed 11 times enhancement of the X-ray output in the half-cavity configuration in comparison to the single pass provides a clear evidence that the laser is deeply saturated. Thus, in contrast to the pump laser the XRL is more stable.

Other XRL beam parameters like intensity, energy, pulse duration, and coherence, respectively are objects of further investigations. However, the pointing angle of the XRL beam is almost identical for the single-pass shots as well as for the half-cavity shots having a value around 5 mrad in relation to the target surface. For this quite stable parameter a chi-squared test makes no sense. Indeed, the pointing angle is only stable for re-injection angles between 1 and 5 mrad [38]. It is surprising that these rather small re-injection angles enable the half-cavity to compensate the XRL beam refraction after the first pass. By way of contrast a wide scattering of deflection angles was observed in [27,44] for the TCE nickel-like Ag laser evaluating altogether 15 (single-pass) shots under traveling-wave irradiation. Thus the in this work observed stability seems to be related to the high-gain region in the plasma due to the saturation in the specific half-cavity configuration. To clarify the details of the gain-profile it is planned to improve the diagnostics by installing a near-field imaging system.

Table 3. Parameters of the 21.2-nm beam emitted by the half-cavity. The beam symmetry shows a narrow Gaussian distribution.

Wavelength	21.22 nm
Output pulse energy (max.)	4 mJ
Number of photons per pulse	$\sim 4 \times 10^{14}$
Mean beam divergence ($h \times v$)	3.5×4.8 mrad
Stand. deviation of divergence ($h \times v$)	0.9×1.3 mrad
Beam symmetry (h/v)	0.75
Stand. deviation of symmetry	0.25
No. of shots with one Mo/Si mirror	~ 100
Pointing angle (resp. to target surface)	$5(\pm 0.5)$ mrad

6 Summary

Double-pass amplification of a Ne-like zinc soft X-ray laser emitting at 21.2 nm is reported, together with a statistical study of its beam quality. The presented half-cavity based X-ray laser at 21.2 nm delivers stable output parameters over a long series of XRL shots. We made a statistical analysis over 110 shots during the two-week experimental period as well over 18 shots during a single day. A chi-squared fitting test procedure allows to have some trust into the hypothesis that the divergence is normally (Gaussian) distributed and almost independent from other controllable parameters like the re-injection angle of the half-cavity mirror [38].

The 450-ps duration of the pump pulse has been found to be adequate to maintain the population inversion over the whole roundtrip in the 38.5-mm long half-cavity [38]. The half cavity can be driven routinely without exchange of any component. Protecting the not used mirror surface by shielding from debris we are able to perform up to 100 shots in a series using one single mirror.

The main characteristics of the half-cavity zinc XRL are summarised in Table 3.

High reproducibility and stability recommend this type of X-ray laser as a robust tool for future applications. By using the half-cavity the XRL emission emerges as a narrow divergent beam possessing a high spatial quality stable over more than 110 shots in a series. The stable beam quality makes future applications possible applying 3 shots per hour of high reproducibility. As a precursor application, we have successfully exploited this laser at PALS for interferometric probing of solid state surfaces related to a strong electrical field [41]. It is planned to reserve some X-ray laser beam time for external research groups.

The chi-squared tests performed in this work are giving no statistical significance to reject the hypothesis of a Gaussian distribution for the small fluctuations seen during a series of 18 shots achievable in one day at maximum. Nevertheless, it is clear that the statistics will be improved with increasing number of shots. Thus for the application experiments projected in the near future it is planned to continue the beam diagnostics and the statistical analysis. In conclusion, the narrow distribution in the scattering of the XRL beam quality in comparison to the rather wide-distributed fluctuations of the pump laser energy illustrates a considerable stability of the half-cavity Zn XRL.

The authors thank the PALS facility staff for providing excellent support for this experiment. We thank J. Moravec (Foton, Nova Paka, Czech Rep.) for implementation of the X-ray CCD. Fundamental support of K. Rohlena, J. Ullschmied, and K. Jungwirth is greatly appreciated. The multilayer mirrors were fabricated by J. Sobota of the Institute of Scientific Instruments (Brno, Czech Rep.). This work was financed partially from the EU Transnational Access to Research Infrastructures Grant HPRI-00108, from the National Research Centres Project LN00A100, and from the Czech Academy of Sciences Grant A1010014.

References

1. X-ray Lasers 2000, *Proceedings of the 7th International Conference on X-ray Lasers*, edited by G. Jamelot, C. Möller, A. Klisnick, J. Phys. IV France **11**, Pr2 (2001)
2. J.J. Rocca, Rev. Sci. Instrum. **70**, 3799 (1999)
3. B.J. MacGowan, L.B. DaSilva, D.J. Fields, C.J. Keane, J.A. Koch, R.A. London, D.L. Matthews, S. Maxon, S. Mrowka, A.L. Osterheld, J.H. Scofield, G. Shimkaveg, J.E.T rebes, R.S. Walling, Phys. Fluids B **4**, 2326 (1992)
4. A. Carillon, H.Z. Chen, P. Dhez, L. Dwivedi, J. Jacoby, P. Jaeglé, G. Jamelot, J. Zhang, M.H. Key, A. Kidd, A. Klisnick, R. Kodama, J. Krishnan, C.L.S. Lewis, D. Neely, P. Norreys, D. O'Neill, G.J. Pert, S. Ramsden, J.P. Raucourt, G.J. Tallents, J. Uhomoibhi, Phys. Rev. Lett. **68**, 2917 (1992)
5. L.B. DaSilva, B.J. MacGowan, S. Mrowka, J.A. Koch, R.A. London, D.L. Matthews, J.H. Underwood, Opt. Lett. **18**, 1174 (1993)
6. A.R. Präg, F. Löwenthal, R. Tommasini, J.E. Balmer, Appl. Phys. B **66**, 562 (1998)
7. Y. Li, G. Pretzler, E.E. Fill, Phys. Rev. A **51**, R4341 (1995)
8. Y. Li, G. Pretzler, E.E. Fill, Phys. Rev. A **52**, R3433 (1995)
9. A.R. Präg, F. Löwenthal, J.E. Balmer, Phys. Rev. A **54**, 4585 (1996)
10. J. Zhang, A.G. MacPhee, J. Lin, E. Wolfrum, R. Smith, C. Danson, M.H. Key, C.L.S. Lewis, D. Neely, J. Nilsen, G.J. Pert, G.J. Tallents, J.S. Wark, Science **276**, 1097 (1997)
11. S. Sebban, H. Daido, N. Sakaya, Y. Kato, K. Murai, H. Tang, Y. Gu, G. Huang, S. Wang, A. Klisnick, P. Zeitoun, F. Koike, H. Takenaka, Phys. Rev. A **61**, 043810 (2000)
12. S.J. Topping, R. Keenan, C.L.S. Lewis, Y. Abou Ali, G.J. Tallents, M. Notley, D. Neely, Central Laser Facility RAL Annual Report (2000/2001), pp. 45-46
13. P.V. Nickles, V.N. Shlyaptsev, M. Kalashnikov, M. Schnürer, I. Will, W. Sandner, Phys. Rev. Lett. **78**, 2748 (1997)
14. P.J. Warwick, C.L.S. Lewis, M.P. Kalashnikov, P.V. Nickles, M. Schnürer, A. Behjat, A. Demir, G.J. Tallents, D. Neely, E. Wolfrum, J. Zhang, G.J. Pert, J. Opt. Soc. Am. B **15**, 1808 (1998)
15. R.E. King, G.J. Pert, S.P. McCabe, P.A. Simms, A.G. MacPhee, C.L.S. Lewis, R. Keenan, R.M.N. O'Rourke, G.J. Tallents, S.J. Pestehe, F. Strati, D. Neely, R. Allott, Phys. Rev. A **64**, 053810 (2001)

16. A. Klisnick, J. Kuba, D. Ros, R. Smith, G. Jamelot, C. Chenais-Popovics, R. Keenan, S.J. Topping, C.L.S. Lewis, F. Strati, G.J. Tallents, D. Neely, R. Clarke, J. Collier, A.G. MacPhee, F. Bortolotto, P.V. Nickles, K.A. Janulewicz, Phys. Rev. A **65**, 033810 (2002)
17. J. Dunn, Y. Li, A.L. Osterheld, J. Nilsen, J.R. Hunter, V.N. Shlyaptsev, Phys. Rev. Lett. **84**, 4834 (2000)
18. Y. Li, J. Dunn, J. Nilsen, T.W. Barbee, A. Osterheld, V.N. Shlyaptsev, J. Opt. Soc. Am. B **17**, 1098 (2000)
19. J.J. Rocca, D.P. Clark, J.L.A. Chilla, V.N. Shlyaptsev, Phys. Rev. Lett. **77**, 1476 (1996)
20. G. Tomassetti, A. Ritucci, A. Reale, L. Palladino, L. Reale, S.V. Kukhlevsky, F. Flora, L. Mezi, J. Kaiser, A. Faenov, T. Pikuz, Eur. Phys. J. D **19**, 73 (2002)
21. B.E. Lemoff, G.Y. Yin, C.L. Gordon, C.P.J. Barty, S.E. Harris, Phys. Rev. Lett. **74**, 1574 (1995)
22. J. Nilsen, B.J. MacGowan, L.B. DaSilva, J.C. Moreno, Phys. Rev. A **48**, 4682 (1993)
23. B. Rus, A. Carillon, B. Gauthé, P. Goedtkindt, P. Jaeglé, G. Jamelot, A. Klisnick, A. Sureau, P. Zeitoun, J. Opt. Soc. Am. B **11**, 564 (1994)
24. E.E. Fill, Y. Li, D. Schlögl, J. Steingruber, J. Nilsen, Opt. Lett. **20**, 374 (1995)
25. B. Rus, A. Carillon, P. Dhez, P. Jaeglé, G. Jamelot, A. Klisnick, M. Nantel, P. Zeitoun, Phys. Rev. A **55**, 3858 (1997)
26. B.R. Benware, C.H. Moreno, D.J. Burd, J.J. Rocca, Opt. Lett. **22**, 796 (1997)
27. J. Kuba, A. Klisnick, D. Ros, G. Jamelot, P. Fourcade, J.-L. Miquel, S. Jacquemot, N. Blanchot, J.-F. Wyart, J. Phys. IV France **11**, Pr2-35 (2001)
28. J.E. Balmer, M. Braud, F. Loewenthal, J. Phys. IV France **11**, Pr2-137 (2001)
29. H.J. Tang *et al.*, J. Phys. IV France **11**, Pr2-129 (2001)
30. J. Nilsen, *Proceedings of the 6th Int. Conference on X-ray Lasers*, edited by Y. Kato, H. Takuma, H. Daido, IOP Conf. Ser. **159**, 475 (1999)
31. C.H. Moreno, M.C. Marconi, V.N. Shlyaptsev, B.R. Benware, C.D. Macchietto, J.L.A. Chilla, J.J. Rocca, A.L. Osterheld, Phys. Rev. A **58**, 1509 (1998)
32. P. Fourcade, D. Ros, P. Zeitoun, D. Benredjem, A. Carillon, S. Hubert, A. Klisnick, G. Jamelot, J. Phys. IV France **11**, Pr2-147 (2001)
33. S.J. Weng *et al.*, Jpn J. Appl. Phys. **37**, L1234 (1998)
34. H. Daido, S. Sebban, N. Sakaya, Y. Tohyama, Y. Norimatsu, K. Mima, Y. Kato, S. Wang, Y. Gu, G. Huang, H. Tang, K. Murai, R. Butzbach, I. Uschmann, M. Vollbrecht, E. Förster, J. Opt. Soc. Am. B **16**, 2295 (1999)
35. J.F. Kenney, E.S. Keeping, *Mathematics of Statistics*, 2nd edn. (Princeton, NJ, Van Nostrand, 1951), Part 2
36. B. Rus, T. Mocek, A.R. Präg, J.C. Lagron, M. Hudeček, G. Jamelot, K. Rohlena, J. Phys. IV France **11**, Pr2-589 (2001)
37. K. Jungwirth, A. Cejnarova, L. Juha, B. Kralikova, J. Krasa, E. Krousky, P. Krupickova, L. Laska, K. Masek, T. Mocek, M. Pfeifer, A. Präg, O. Renner, K. Rohlena, B. Rus, J. Skala, P. Straka, J. Ullschmied, Phys. Plasmas **8**, 2495 (2001)
38. B. Rus, T. Mocek, A.R. Präg, M. Kozlová, G. Jamelot, A. Carillon, D. Ros, D. Joyeux, D. Phalippou, Phys. Rev. A (accepted, 2002)
39. W. Chen, S. Wang, B. Chen, A. Xu, C. Mao, Chin. Phys. **12**, 403 (1992)
40. A. Carillon, P. Dhez, B. Gauthé, P. Jaeglé, G. Jamelot, A. Klisnick, J.C. Lagron, SPIE Proc. **1140**, 271 (1989)
41. L. LeDeroff, P. Salieres, B. Carre, D. Joyeux, D. Phalippou, Phys. Rev. A **61**, 043802 (2000)
42. A.G. MacPhee, C.L.S. Lewis, P.J. Warwick, I. Weaver, P. Jaeglé, A. Carillon, G. Jamelot, A. Klisnick, B. Rus, P. Zeitoun, M. Nantel, P. Goedtkindt, S. Seban, G.J. Tallents, A. Demir, M. Holden, J. Krishnan, Opt. Commun. **133**, 525 (1997)
43. D.B. Owen, *Handbook of statistical tables* (Reading MA, Palo Alto, London, Addison-Wesley, 1962)
44. J. Kuba, A. Klisnick, D. Ros, P. Fourcade, G. Jamelot, J.-L. Miquel, N. Blanchot, J.-F. Wyart, Phys. Rev. A **62**, 043808 (2000)